

Accounts

Vibrational Energy Relaxation of Metalloporphyrins in a Condensed Phase Probed by Time-Resolved Resonance Raman Spectroscopy

Yasuhisa Mizutani[#] and Teizo Kitagawa[*,†]

Institute for Molecular Science, Okazaki National Research Institutes, Myodaiji, Okazaki 444-8585

†Center for Integrative Bioscience, Okazaki National Research Institutes, Myodaiji, Okazaki 444-8585

(Received July 2, 2001)

Recent experimental work on vibrational energy relaxation of metalloporphyrins in a condensed phase carried out in this laboratory is summarized. The formation of a vibrationally excited photoproduct of metalloporphyrins upon (π, π^*) excitation and its subsequent vibrational energy relaxation were monitored by picosecond time-resolved resonance Raman spectroscopy. Results related to intramolecular relaxation of octaethylporphyrinato nickel (NiOEP) are described. Stokes Raman bands due to a photoproduct of NiOEP instantaneously appeared upon the photoexcitation. Their intensities decayed with a time constant of ~300 ps, which indicates an electronic relaxation from the (d, d) excited state (B_{1g}) to the ground state (A_{1g}), being consistent with the results of transient absorption measurements. Anti-Stokes ν_4 and ν_7 bands for vibrationally excited (d, d) state of NiOEP decayed with time constants of ~10 and ~300 ps. The former is ascribed to vibrational relaxation, while the latter corresponds to the electronic relaxation from the (d, d) excited state to the electronic ground state. While the rise of anti-Stokes ν_4 intensity was instrument-limited, the rise of anti-Stokes ν_7 intensity was delayed by 2.0 ± 0.4 ps, which indicates that intramolecular vibrational energy redistribution has not been completed in the subpicosecond time regime. To study the mechanism of intermolecular energy transfer, solvent dependence of the time constants of anti-Stokes kinetics was investigated using various solvents. No significant solvent dependence of the rise and decay constants was observed for NiOEP. For an iron porphyrin, we observed two phases in intermolecular energy transfer. The fast phase was insensitive to solvent and the slow phase depended on solvents. A model of classical thermal diffusion qualitatively reproduced this behavior. For myoglobin, temporal changes of the anti-Stokes Raman intensity of the ν_4 and ν_7 bands demonstrated immediate generation of a vibrationally excited heme upon photodissociation and subsequent decays of the excited populations, whose time constants were 1.1 ± 0.6 and 1.9 ± 0.6 ps, respectively. This direct monitoring of the cooling dynamics of the heme cofactor within the protein matrix allows the characterization of the vibrational energy flow through the protein moiety and to the water bath. For solute–solvent energy transfer process, low-frequency modes of proteins seem to be less important.

A principal physical model for chemical dynamics in solution is provided by the motion of atoms under the influence of potential energy curves in the presence of solvent molecules that exchange and dissipate the energy and momentum of solute. This picture was first presented by Kramers in 1940; it employs a model for the reaction coordinate dynamics described by the Langevin equation, in which the force acting on the Brownian particle at any instant is assumed to consist of two parts: a frictional force and a randomly fluctuating force. The friction and force fluctuations are related by the fluctuation–dissipation theorem. Vibrational energy relaxation (VER) can be viewed as the dissipative process of non-equilibrium vibrational energy due to the forces exerted by the bath on motion of atoms along the molecular vibrational coordinate. The bath mode can be the modes of solvents or, for polyatomic molecules, the rest of the molecular degrees of freedom that do not constitute the reaction coordinate. The former includes intermolecular energy transfer (IET), while the latter includes intramolecular vibrational energy redistribution (IVR).

Numerous processes in condensed phases involve dissipation of energy from vibrationally excited modes. Accordingly, VER has attracted much attention.[1–3] Upon photoexcitation, excess energy is initially deposited in Franck–Condon active vibrations. Right after nonradiative transition, the energy is localized in so-called "accepting" and "promoting" modes.[4–6] Subsequent thermal equilibration processes are not fully understood for the excited molecules in solutions. In a picture for a polyatomic molecule in gas phase, the energy relaxation process would be composed of two temporally distinct steps: IVR among all vibrational freedoms of the molecule and IET to other molecules by collisions and the like. For large mole-

Present address: Molecular Photoscience Research Center, Kobe University, Nada, Kobe 657-8501

cules in solution, the collision rates are of the order of 10^{12} s^{-1}, which is close to the time scale of IVR, and this brings about complex evolutions of vibrational population.[7]

Recently, the evolutions of vibrational populations of many fundamentals were studied in detail for small molecules; they showed mode-specific intermolecular vibrational energy transfer,[8–10] which indicates that the two steps are not temporally distinct. For large molecules in solution, however, the time scales of IVR and IET are not clear due to lack of detailed studies. IET is found to occur on the time scale of 1–100 ps, while IVR is generally believed to occur on the subpicosecond time scale for large molecules in solution,[3,11] without clear experimental evidence. Standard theoretical descriptions of solution phase reactions such as RRKM theory employ the reaction coordinate picture, in which modes orthogonal to the reactive motion are considered to remain in statistical distribution with one another and also with modes of the solvent during the course of the reaction. While this may be a good approximation on the time scale of activated process in which IVR is faster compared with barrier crossing, it is not expected to hold in the reactions with low or no barrier. In such cases, the motion along the reaction coordinate can occur on time scales comparable to IVR, or even faster. Thus, for barrier crossing phenomena in solution, the rate for coupling energy into the reaction coordinate relative to those for energy transfer to the solvent and to other unreactive modes of the excited molecule may determine the rate, pathway, and efficiency of a given reaction. Therefore, a microscopic understanding of solvent-induced vibrational relaxation processes is essential to provide a detailed picture of chemical reactions.

Vibrational relaxation dynamics in the condensed phase has been extensively studied with time-resolved pump-probe optical spectroscopy. For example, in the case of VER in the electronic ground state, the solute molecules were vibrationally excited by a picosecond infrared pulse, or were excited indirectly by internal conversion from a higher lying electronic state. The subsequent energy transfer to the solvent was monitored with the thermal broadening of the S_1–S_n absorption or the S_1–S_0 emission spectrum. The thermally enhanced, low frequency tail of the absorption spectrum (or the high energy part of the emission spectrum) arising from electronically and vibrationally excited states gives information on the transient temperature of the vibrational system. The cooling kinetics was derived from time dependent changes of the absorption coefficient or of the emission intensity. This enabled the measurements of the energy flow from the molecule to the solvent. A more sophisticated estimate of the energy distribution can be given by comparison of transient absorption spectra with temperature dependent absorption spectra of the S_0–S_1 transition that were simulated with the Franck-Condon factors of the active modes obtained from their resonance Raman intensities. Using this method, one can roughly estimate the energy distribution and/or the time-dependent internal temperature of the system. It was proposed from this kind of experiment that IVR is not necessarily ultrafast, even for large molecules like stilbene[12,13] or 2-(2-hydroxy-5-methylphenyl)benzotriazole.[14] However, the interesting questions concerning the initial energy distribution and the detailed pathway to a thermal distribution are not easily answered by this kind of experiment, since usually the vibronic structures of the electronic transition are not spectrally resolved for solutions.

Time-resolved Raman and infrared techniques allow, at least in principle, more direct monitoring of vibrational populations because their energy resolution is much higher than visible absorption or emission spectroscopy. In infrared spectroscopy, high resolution in frequency and time can be obtained simultaneously when carefully considering the coherent interaction between the ultrashort probing pulse and the sample,[15,16] since frequency selection by a spectrometer can be incorporated after the light pulse interacts with the molecule. However, it is still a hard task to measure femtosecond or picosecond time-resolved IR spectra in a wide frequency range (300–3000 cm^{-1}), due to the interference of solvent bands and the difficulties in the generation and multichannel detection of broad infrared pulse, although the transient femtosecond IR technique is making recent progress.[17–21] On the other hand, in time-resolved resonance Raman (TR^3) technique, subpicosecond time resolution cannot be compatible with high resolution of frequency, since they are achieved during the same interaction between the light pulse and the molecule. However, time-resolved anti-Stokes Raman spectroscopy is selective for vibrationally excited modes and therefore is powerful to measure VER. This technique has an advantage that many vibrational transitions in a wide frequency range are simultaneously observed with a single probe frequency. Furthermore, the resonance effect allows us to measure the vibrational spectra of solute without severe solvent interference. Due to the high repetition rate of modern Ti:sapphire laser systems, a sufficiently high signal-to-noise ratios can be achieved so as to apply ps-TR^3 experiments to a broad variety of molecules, although the anti-Stokes Raman scattering is very weak. The ratio of the integrated areas of anti-Stokes and Stokes scattering, corrected to the first order for reabsorption and cross section differences, is expected to yield the most direct information about relative vibrational populations,[22,23] and is therefore essential to studies of energy distribution dynamics in molecular systems. Recently picosecond time-resolved vibrational studies on the time scale of IVR have been reported.[24–31] Some of them questioned the assumption that IVR is much faster than IET for large molecules in solution.[25–27,29–31]

In this account, we review our recent experimental studies on VER of metalloporphyrins in condensed phase by using TR^3 spectroscopy. The advantages of metalloporphyrins for the study of VER are described in Sec. 1. The IVR and IET of metalloporphyrins are discussed in Secs. 2 and 3, respectively. Our conclusion will be presented in Sec. 4.

1 Advantages of Metalloporphyrins for the Study of VER

1.1 Suitable Systems for the Study of VER. In order to study VER accompanying a photoreaction, it is very important to make the right choice of molecules and photoreactions in the study. Figure 1(a) schematically illustrates a suitable system for the study of VER. We begin with photoexcitation of a molecule into an electronic excited state (B). In order to obtain large excess energy for the excited molecule, we chose the molecules which show ultrafast transition to another electronic state (C) via nonradiative transition or ultrafast photoreaction, transferring most of the electronic energy into the vibrational

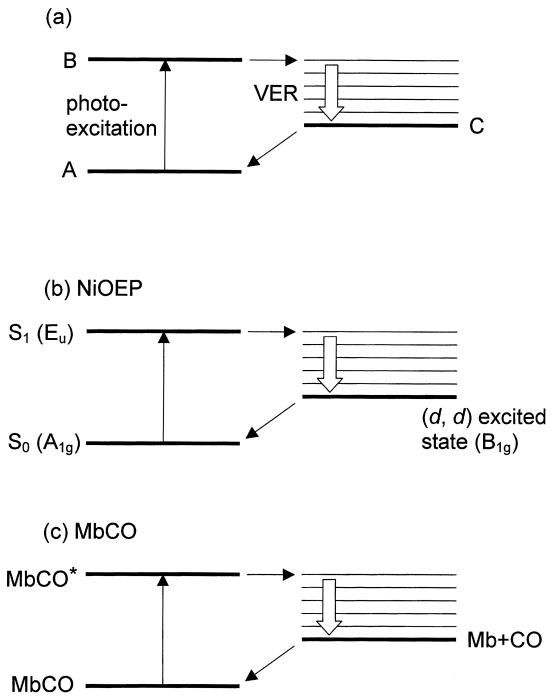

Fig. 1. Suitable system for the study of VER. (a) Schematic description of the suitable system. (b) Photochemistry of NiOEP. (c) Photochemistry of MbCO.

degrees of freedom. This transition of the molecule in the state C has to be complete within a few hundreds of a femtosecond, which is shorter than the instrument response time of the measurement and the IET time. Thus the molecule with large excess energy in the electronic state C can be observed instantaneously upon the photoexcitation. The lifetime of this electronic state must be longer than ~100 ps to have a reasonable temporal separation between electronic and vibrational relaxation so that we have a time window wide enough to monitor VER in the state C. The molecule ends up with the original electronic state A so that the molecule is recyclable.

1.2 Advantages of Metalloporphyrins for the Study of VER. We have been studying the VER of metalloporphyrins in condensed phase. Metalloporphyrins are metal complexes of π-conjugated tetrapyrrole macrocycles. Among a variety of metalloporphyrins, we have chosen octaethylporphyrinato nickel (NiOEP) and heme (iron protoporphyrin IX) in myoglobin (Mb) for the study of VER. For these porphyrins, photoexcited metalloporphyrins exhibit photochemical dynamics as shown in the scheme of Fig. 1(a).

Figure 1(b) illustrates the photochemistry of NiOEP. The photochemistry of NiOEP has been studied by Holten and coworkers with femtosecond transient absorption spectroscopy.[32,33] According to their results, photoexcitation of nickel porphyrins in noncoordinating solvents, such as toluene and benzene, leads to the formation of a relatively long-lived (*d*, *d*) excited state (B_{1g}), via nonradiative transition from the (π, π^*) state (E_u). This nonradiative transition deposits an excess energy of 10,000 cm^{-1} into the vibrational manifold of the macro cycle. The decay of the (*d*, *d*) excited state into the A_{1g} ground state takes place in about 300 ps, allowing reasonable separation on the time scale between expected vibrational relaxations and electronic relaxations. Therefore, the photochemistry of NiOEP meets the requirements described above.

Figure 1(c) illustrates the reaction scheme of MbCO. Ultrafast optical absorption studies[34,35] of MbCO revealed that a ligand bound to the heme in Mb is dissociated upon photoexcitation within 50 fs with a quantum yield of nearly unity. Geminate recombination of O_2, which is a physiological substrate, is fast and occurs in the subnanosecond regime, while that of CO is slow and occurs in the submicrosecond regime. By using CO rather than O_2 as the ligand, it is possible to avoid complicated side reactions and associated population dynamics.

There are additional advantages for metalloporphyrins. Molecular vibrations of metalloporphyrins in the electronic ground state have been well characterized through resonance Raman and IR experiments and normal coordinate analysis.[36–39] The S_0–S_1 (Q band) and S_0–S_2 (B band) absorption bands are reasonably separated and they are suitable to use for resonance bands in pump-probe excitations.

1.3 VER of Metalloporphyrins so far Studied. Little is understood about vibrational dynamics in metalloporphyrins. Spectral congestion and the independence of the fluorescence lifetime from degrees of vibrational excitation have been interpreted as indirect evidence for efficient IVR in the S_1 excited state of jet-cooled metalloporphyrins.[40–44] Studies on vibrational energy dynamics for solvated metalloporphyrins are few. For hemeproteins, there are several time-resolved studies to interrogate the internal dynamics of photoexcited hemes. Petrich et al. observed a frequency shift for photodissociated hemoglobin (Hb) in early picosecond range and ascribed it to an IET process.[45,46] Lingle et al. monitored Stokes and anti-Stokes scattering from photoexcited deoxyHb using TR^3 spectroscopy (8 ps pulse).[47,48] They observed saturation of Stokes scattering and increased anti-Stokes scattering, which decayed in the ~10 ps range and explained the results in terms of the vibrational relaxation of a thermally excited ground state heme. Li et al. estimated IET time constants from nanosecond Raman saturation spectroscopy.[49] Studies of deoxyHb and heme model complexes using ~30 ps pulses by Friedman and co-workers suggested mode selective energy localization during photoexcitation.[50–52] Sato and Kitagawa,[26] and Mizutani et al.[31] reported anti-Stokes spectra of NiOEP and suggested that the energy randomization may not be completed on a subpicosecond time scale. Recently, Mizutani and Kitagawa directly observed the cooling process of heme upon photodissociation of carbonmonooxy Mb.[53]

2 Experimental

Picosecond time-resolved resonance Raman (ps-TR^3) spectroscopy is a promising technique to investigate the ultrafast structural changes of molecules.[54] Nevertheless, ps-TR^3 spectroscopy is not implemented as widely as nanosecond TR^3 spectroscopy because of practical limitations. The most crucial factor is lack of a light source that fulfills the requirements for small timing jitters, appropriate repetition rates, and the wavelength tunability of pulses applicable to ps-TR^3 spectroscopy, which requires two beams: a pump beam to photoexcite molecules of interest and a probe beam to monitor the subsequent changes occurring in the excited or reacted molecules. To obtain the TR^3 spectra of a wide variety of molecules with

high S/N ratios within a reasonable measuring time, it is quite important to use two independently tunable light sources with a high repetition rate for the pump and probe beams. Repetition rates in the kilohertz range are desirable for practical purposes, but so far, no one has succeeded in observing ps-TR^3 spectra with a widely tunable pulse source at kilohertz repetitions. We constructed an apparatus consisting of widely tunable light sources for ps-TR^3 spectroscopy using a 1-kHz picosecond Ti:sapphire laser/regenerative amplifier system.[55]

Details of experimental procedures were described elsewhere.[56] A picosecond mode-locked Ti:sapphire oscillator (Spectra-Physics, Tsunami 3950), pumped by an Ar^+ ion laser (Spectra-Physics, BeamLok 2060), produced approximately 1.5-ps pulses with a repetition of 82 MHz and an average power of about 0.7 W. The seed pulse was amplified by a regenerative amplifier (Positive Light, Spitfire) operated at 1 kHz by pumping with the 527-nm output of an intracavity frequency-doubled Nd:YLF laser. This amplification unit provides ~780-nm pulses, each with an energy of about 0.8 mJ, duration of 2.5 ps, and spectral width of 6 cm^{-1} in a nearly TEM_{00} mode under operation at 1 kHz. A visible pump pulse was generated with a home-built optical parametric generator (OPG) and amplifier (OPA), which were pumped with the second harmonic of the laser output. A probe pulse was generated as the first Stokes stimulated Raman scattering from compressed methane gas (50 kg/cm^2) excited by the second harmonic of the laser output. The pump and probe beams were made collinear and coaxial using a dichroic mirror. The polarization of the pump beam was rotated by 55° relative to that of the probe beam to minimize the effects of molecular rotations on the observed kinetics. The cross correlation width of the pump and probe pulses was measured with a 1-mm BBO crystal to be 2.3 ps. The 0.0 ps of delay time (uncertainty < 0.2 ps) was calibrated using sum frequency mixing in the same crystal.

The sample solution was placed in a 10-mmϕ NMR tube and spun with a spinning cell device that was designed to minimize the off-center deviation during rotation.[57] The sample was spun at 3400 rpm in the spinning cell configured for 135° back-scattering illumination and collection. This configuration is important to minimize the effects of molecular rotations on the observed kinetics.[58] Spherical and cylindrical lenses were used to focus the pump and probe beams on the sample. In ps-TR^3 experiments, it is very important to use weak probe power. The probe power was empirically selected so that the sample had no anti-Stokes ν_4 band of the photoproduct in the probe-only spectrum.[56]

Raman scattering was collected by a doublet achromat (80-mm focal length (FL), *f*/2) and the beams were imaged onto the 200-μm entrance slit of a single spectrometer (Spex, 500M) by a doublet achromat (200-mm FL, *f*/5). A dichroic short-pass filter was placed between the lenses to remove the scattered pump beam. A holographic notch filter (Kaiser Optical Systems) was used to reject the unshifted scattering. A polarization scrambler was placed at the entrance slit to remove the effects of polarization on the spectrograph throughput. The spectrograph is equipped with a blazed-holographic grating (2400 grooves/mm) that enables measurements of a spectrum as wide as about 1000 cm^{-1} in the Soret region and with a spectral slit width of approximately 8 cm^{-1}. The dispersed light was detected by a liquid-nitrogen-cooled CCD detector (Princeton Instruments, CCD-1100PB). Raman shifts were calibrated with cyclohexane, benzene, or carbon tetrachloride. The peak positions of Raman bands are accurate within ±2 cm^{-1}.

NiOEP, iron(III) protoporphyrin IX (FePPIX) (Aldrich Chemical Co.), *meso*-tetrakis(4-sulfonatophenyl)porphyrinato iron(III) (FeTSPP) (Porphyrin Products) and horse skeletal Mb (Sigma, M-0630) were used without further purification. All solvents used were of spectroscopic grade (Dojindo Laboratories).

3 IVR of Metalloporphyrins

3.1 Ni Porphyrins. Figure 2 shows Stokes-TR^3 spectra of the NiOEP photoproduct in benzene. The delay times of the probe pulse from the pump pulse are indicated at the left side of each spectrum. In these spectra, the contribution of unreacted species has been subtracted and signal intensities are corrected using the intensities of solvent bands (993 cm^{-1}) to eliminate the effect of self-absorption of the sample. The

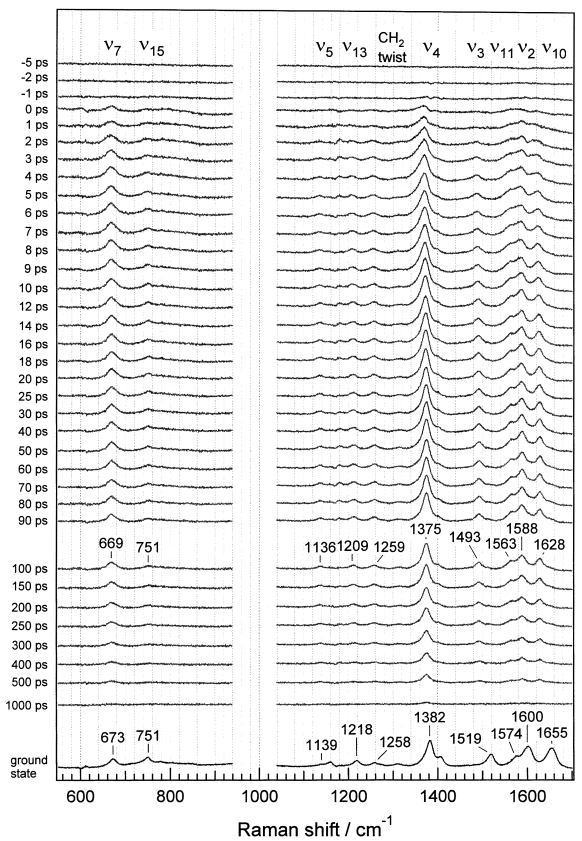

Fig. 2. Stokes TR^3 spectra of photoproduct of NiOEP in benzene. The pump-probe delay times are indicated at the left side of each spectrum. In these spectra the contribution from unreacted species has been subtracted and signal intensities are corrected using the intensities of solvent bands (992 cm^{-1}) to eliminate the effect of self-absorption of the sample. The probe-without-photolysis spectrum is given at the bottom of the figure for comparison (pump: 556 nm, probe: 435 nm).

probe-without-photolysis spectrum (ground state spectrum) is given at the bottom of the figure for comparison.

In negative delay times, the difference spectra are absolutely featureless, and this corroborates the present measurement of cross correlation width of 2.3 ps. In positive delay times new bands appeared, which meant the generation of a photoproduct. Their intensities increased up to 4 ps, and then gradually decreased with time. At 1 ns of delay time the difference spectrum was absolutely featureless, indicating that the photoproduct has completely turned into the ground-state species. The bands of the 100-ps delay spectrum at 669, 751, 1136, 1209, 1259, 1375, 1493, 1563, 1588, and 1628 cm^{-1} are assigned to ν_7, ν_{15}, ν_5, ν_{13}, CH_2 twist, ν_4, ν_3, ν_{11}, ν_2, and ν_{10} modes, respectively, on the basis of the ground state spectra.[59] The observed Raman spectra are consistent with those reported previously for the ground state species[36,38] and the photoproduct.[26,60]

Stokes RR intensities provide us information on the population of the photoproduct, because they are proportional to the number of molecules if the intensities are corrected for the effect of self absorption. To see the intensity change quantitatively, the Stokes ν_4 band intensities are plotted against the delay time in Fig. 3 (circles), where the lower panel shows the expanded plot between −5- and 100-ps delay. In the curve fitting calculations, the system response was deconvoluted from the Stokes intensity change using a Gaussian fit (the corresponding cross correlation width is 2.3 ps) to the cross-correlation signal. This temporal change is well described with a single exponential decay with a time constant of 330 ± 40 ps, as is shown with a solid curve in Fig. 3. This number is close to the lifetime of the (*d*, *d*) excited state of NiOEP reported by Kim et al.[32] The rising part indicates that ν_4 band appeared promptly within the instrument response time, consistent with the fact that nonradiative transition from the (π, π^*) excited state to the (*d*, *d*) excited state occurs in less than 350 fs.[33] Solid squares in Fig. 3 show temporal profiles of ν_7 band. This band also shows essentially the same temporal profile as that of the Stokes ν_4 band. Therefore, the Stokes intensity decays reflect the population decay of the (*d*, *d*) excited state of NiOEP. Moreover, the observed frequency differences for ν_2, ν_3, ν_{10}, and ν_{11} bands between the (*d*, *d*) excited state and the electronic ground state are well interpreted with the idea of core expansion of the porphyrins by about 0.05 Å.

Peak positions of the Stokes bands in Fig. 2 gradually shifted upward until 20 ps, accompanied by band narrowing. Such changes in the band shape as well as in the band intensity are important to understand ultrafast processes after the nonradiative transition. The changes of the Stokes bands are well described by single exponential functions with time constants of 9.2 ± 1.3 ps for the peak position and 8.3 ± 3.7 ps for the bandwidth. These are totally different from the electronic lifetime and are not associated with the electronic relaxation. Therefore, this frequency shift can be attributed to other photophysical process such as IET. In fact, both time constants are close to the IET time estimated from anti-Stokes intensity decay of ν_4 and ν_7 bands (vide infra). Therefore, this frequency shift and band narrowing should be something associated with IET. Similar spectral evolution associating with IET has been observed for *trans*-stilbene,[24,61–63] *trans*-4, 4′-diphenylstilbene,[25] azobenzene,[64] Mb,[53] Hb,[45,46] and NiOEP.[26,31] One may

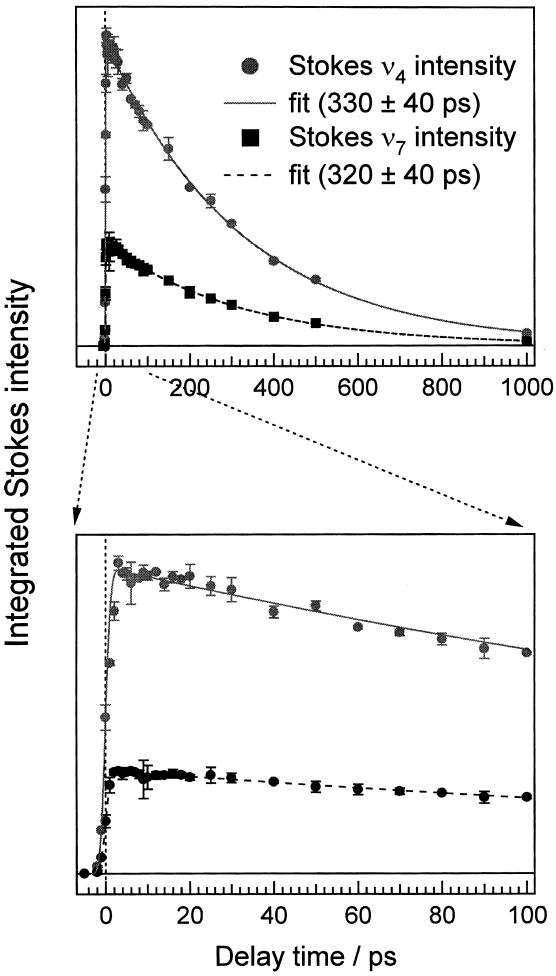

Fig. 3. Temporal change of the Raman intensity of the Stokes ν_4 (circles) and ν_7 bands (squares) of NiOEP in the (*d*, *d*) excited state. The lines represent the results calculated for instantaneous rise followed by a single exponential decay convoluted with a Gaussian instrument response function for which the cross correlation time is 2.3 ps. The best fit was obtained by decay time constants of 330 ± 20 ps for ν_4 band and 320 ± 40 ps for ν_7 band, respectively. The lower panel shows a closeup of the curve in the early time region.

interpret the time-dependent increases in the ν_4 and ν_7 frequencies of the photoproduct as being due to intermolecular vibrational relaxation causing depopulation of higher levels in an anharmonic potential surface. Given the limited population at vibrational levels greater than v = 1, the observed frequency evolution is much larger than that normally expected for exclusively thermal relaxation of anharmonic oscillators. In other words, we would have to assume unreasonably large anharmonicity and anomalously large Raman cross section for v = 1 → 2 transition relative to that for v = 0 → 1 transition for the ν_4 mode to explain the observed shift if we adhere to this model.

A second possibility is that the frequency evolution is due to anharmonic coupling between the ν_4 mode and low-frequency porphyrin modes. Hamm et al. proposed the alternative model in which anharmonic couplings of the high-frequency mode with the bath of the remaining low-frequency modes are as-

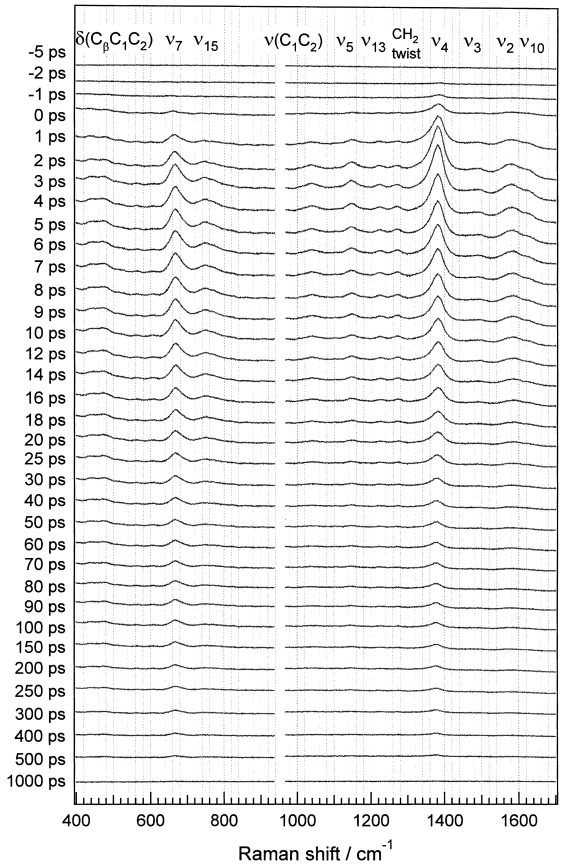

Fig. 4. Anti-Stokes TR^3 spectra of the photoproduct of NiOEP in benzene. The pump-probe delay times are specified at the left side of each spectrum. In these spectra signal intensities are corrected using the intensities of solvent bands (992 and 607 cm^{-1}) to eliminate the effect of self-absorption of the sample (pump: 556 nm, probe: 435 nm).

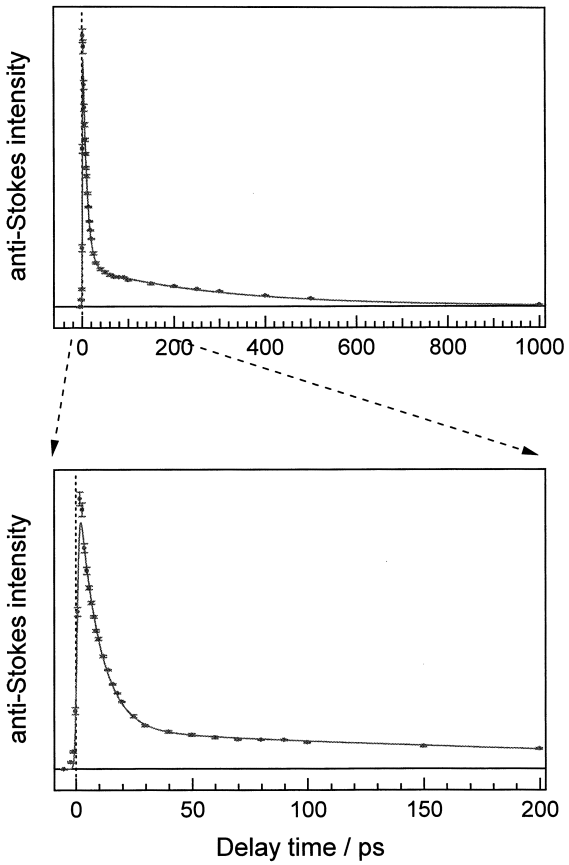

Fig. 5. Temporal change of the Raman intensity of the anti-Stokes ν_4 band of NiOEP in the (d, d) excited state. The data were fit to a double exponential function of the form, $A \exp(-t/\tau_2)(\exp(-t/\tau_1) + B)$ (an instantaneous rise and a double exponential decay) convoluted with an instrument function as described in the caption of Fig. 3. The curve shown in this figure was obtained with parameters of $\tau_1 = 9.5 \pm 1.2$ ps, $\tau_2 = 340 \pm 50$ ps, and $B = 0.14 \pm 0.02$. The lower panel shows a closeup of the curve in the early time region.

sumed.[64] They showed that off-diagonal anharmonicity between the investigated high-frequency mode and the remaining low-frequency modes dominates the observed transient absorbance changes, while the anharmonicity of the high-frequency mode themselves (diagonal anharmonicity) causes only minor effects. According to their formulation, the transition frequency from v = 0 to v = 1 levels can be changed according to total contribution of the vibrationally excited population of some low-frequency modes. This model, therefore, explains the observed frequency shift whose time constant is similar to that of IET as observed in the present study.

Figure 4 shows anti-Stokes TR^3 spectra on the same photochemical event. Similar to Stokes spectra new bands appear upon photoexcitation by the pump pulse, but their intensity decays are much faster than those of Stokes bands. In order to see the temporal behavior of the anti-Stokes ν_4 band, the Raman intensity change is plotted in Fig. 5. The upper panel shows the plot for the entire time range between -5 and 1000 ps, while the lower panel shows its close-up for the time region between -5 and 200 ps. Clearly there are two decay components. Best fit to the data by a double exponential yielded the decay constants of 9.5 ± 1.2 and 340 ± 50 ps. The slow component can be attributed to the electronic relaxation, because the comparable time constant was also seen in the decay of Stokes bands. The fast component should be ascribed to vibrational energy relaxation, because there is no such component in Stokes spectra. Concerning the intensity rise, ν_4 anti-Stokes band shows the instrument-limited rise, same as the Stokes counterpart.

Figure 6 shows the temporal change of the Raman intensity of the anti-Stokes ν_7 band of NiOEP. The upper panel shows the plot for the time range between -5 and 1000 ps, while the lower panel shows its close-up for the time region between -5 and 200 ps. Similar to the anti-Stokes ν_4 band intensity, this band exhibits biphasic change. The two time constants are almost the same as those of ν_4 band. Contrary to the anti-Stokes ν_4 band, however, this band exhibits a delay in intensity rise. It was impossible to fit the observed data satisfactorily without introducing a rise component. The best fit was obtained with the rise time constant of 2.0 ± 0.4 ps.

Thus, we observed the difference in the intensity rise between anti-Stokes ν_4 and ν_7 Raman bands. One may naively

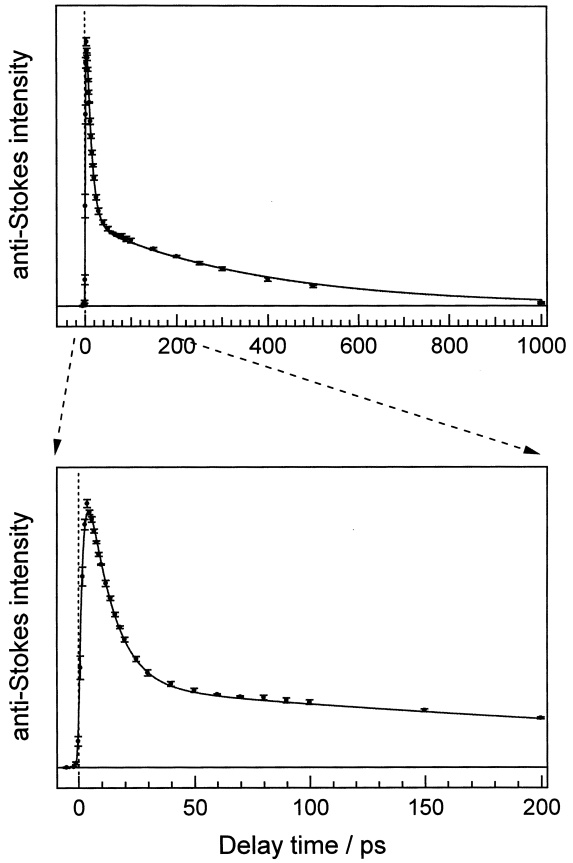

Fig. 6. Temporal change of the Raman intensity of the anti-Stokes ν_7 band of NiOEP in the (d, d) excited state. The data were fit to a double exponential function of the form, $A \exp(-t/\tau_2)\{(\exp(-t/\tau_1) + B) - (1 + B) \exp(-t/\tau_{rise})\}$ (a rise and a double exponential decay) convoluted with an instrument function as described in the caption of Fig. 3. In the function, the component of $\{(\exp(-t/\tau_1) + B) - (1 + B) \exp(-t/\tau_{rise})\}$ describes the populational change in vibrationally excited states with a decay time constant, τ_1, a rise constant, τ_{rise}, and an offset related to an equilibrium value, B. The curve shown in this figure was obtained with parameters of $\tau_{rise} = 2.0 \pm 0.4$ ps, $\tau_1 = 10.8 \pm 1.8$ ps, $\tau_2 = 330 \pm 40$ ps, and $B = 0.26 \pm 0.03$. Note that the rise component was required to fit the rising part of the intensity change. The lower panel shows a closeup of the curve in the early time region.

imagine that all Raman bands of a single molecular species synchronously change their intensities. But this is not true for the case of anti-Stokes scattering because it reflects the vibrational populations of individual modes. The observed delay in the rise time of anti-Stokes ν_7 band is the most direct indication of the difference in evolution of vibrational population among the modes, i.e. IVR processes. To our best knowledge, this is the first observation of a difference in anti-Stokes intensity rises for large molecules in solutions, although a similar difference among the intensity rises of anti-Stokes bands has been observed for naphthalene, which is a rather small molecule.[65]

We have proposed two possible reasons to account for the difference in the intensity rise. One is an effect of population in the higher vibrational levels of the ν_7 mode (intramode randomization), and the other is the transfer of excess energy into the ν_7 mode via other modes (intermode randomization).

The intramode randomization model takes it into consideration that anti-Stokes Raman bands for high vibrational levels are possibly less intensity-enhanced via the resonance effect. In the case of resonance Raman scattering, the Raman cross sections are not the same between the transition of $v = 2 \rightarrow 1$ (and also high $v' \rightarrow v' - 1$) and that of $v = 1 \rightarrow 0$. The anti-Stokes Raman excitation profile is highly dependent on the initial vibrational level of the Raman transition due to the energy denominator term of the polarizability derivative. Therefore if the cross section for $v = 2 \rightarrow 1$ is much smaller than that for $v = 1 \rightarrow 0$, the intensity rise of the anti-Stokes ν_7 band can be delayed: the population at $v = 1$ first increases because of the relaxations from the levels higher than $v = 1$ and then decreases due to the relaxation into the $v = 0$ level. However, the cross section for $v = 2 \rightarrow 1$ is larger than that for $v = 1 \rightarrow 0$ in the first-order expressions for resonance-enhanced Raman cross sections derived by Champion and co-workers.[23] They showed that the expressions are valid for the heme in proteins where, in general, the vibrational modes of the heme are weakly coupled to the electronic transition. This justification to use the first-order expressions can be applied to NiOEP. Therefore, the assumption of less resonance enhancement of anti-Stokes Raman intensity for higher vibrational levels would be unreasonable and intramode randomization model does not explain the delay in the intensity rise of the anti-Stokes ν_7 band within the framework of the statistical energy distribution.[66]

The intermode randomization model assumes that the delay is due to slow IVR between ν_7 and other modes, as described in the following. Right after the nonradiative electronic relaxation from the (π, π^*) excited state to the (d, d) excited state, molecules should possess the excess energy of 11,000–17,000 cm^{-1}. Since the electronic lifetime of the (π, π^*) excited state is very short (< 350 fs), the molecular vibrations of macrocycle receive the excess energy in this timescale. The excess energy should be initially partitioned among promoting and accepting modes in a non-statistical way, as predicted in the theories for nonradiative transition.[4–6] A difference in the intensity rise can be observed if the initial non-statistical energy distribution is randomized in a picosecond time scale. Namely, the excess energy is mainly populated in the ν_4 mode and other few modes, but less populated in the ν_7 mode at the initial stage. Then, the excess energy flows into the ν_7 mode from the ν_4 or other modes for the randomization in a picosecond time scale and this energy randomization causes the delay in the ν_7 population rise.

We also analyzed the temporal behaviors of anti-Stokes intensities of the eight Raman bands observed. Table 1 summarizes the time constants observed for temporal changes of anti-Stokes intensities: the time constants for the rise, vibrational cooling and electronic relaxation. The observed vibrational modes are categorized into three groups with respect to the symmetry of vibration. The time constants for vibrational cooling and electronic relaxation show almost no mode dependence. On the contrary to that, the time constant of the rise highly depends on the mode, and some bands show delay in intensity rise as the ν_7 band does. In Table 1, we can find two

Table 1. Time Constants of Anti-Stokes Intensity Changes of the (d, d) Excited State of NiOEP

Mode	ν/cm^{-1}	τ_{rise}/ps	τ_1/ps	τ_2/ps
		A_{1g} skeletal modes		
ν_3	1493	< 0.3	10.9 ± 3.4	370 ± 80
ν_4	1375	< 0.3	9.5 ± 1.2	340 ± 50
ν_5	1136	0.7 ± 0.3	9.2 ± 1.2	340 ± 50
ν_7	669	2.0 ± 0.4	10.8 ± 1.8	330 ± 40
		B_{1g} skeletal modes		
ν_{13}	1209	1.1 ± 0.3	11.8 ± 2.0	310 ± 60
ν_{15}	751	2.7 ± 0.5	12.1 ± 1.9	350 ± 50
		Ethyl substituent modes		
CH_2 twist	1259	3.4 ± 1.3	8.4 ± 3.0	390 ± 60
$\nu(C_1$–$C_2)$	1022	1.0 ± 0.3	11.0 ± 1.5	340 ± 50

τ_1: IET time constant, τ_2: electronic relaxation time of the (d, d) excited state, τ_{rise}: rise time constant.

trends in the observed rise time constants. One is that, roughly speaking, the rise is faster for totally symmetric modes than for nontotally symmetric modes and ethyl substituent modes, when modes with similar frequencies are compared. The other trend is that, even among the totally symmetric modes, a delay can be recognized for low frequency modes. These non-uniform intensity rises again indicate that there is a nonstatistical distribution of vibrational populations in the first few picoseconds. This difference would reflect the initial energy distribution right after the nonradiative transition to the (d, d) excited state.

The nonradiative transition has been understood in the framework of the breakdown of the Born–Oppenheimer (BO) approximation. In the non-BO theory, two types of vibrational modes are important: *promoting* and *accepting modes*. A promoting mode mixes the electronic characters of the initial and final states of the nonradiative transition and induces the nonradiative transition by changing its vibrational quantum number. In order to be a promoting mode, the vibrational mode has to have the same symmetry character as that of the cross product of symmetry characters of the initial and final electronic states. An accepting mode serves to provide an energy sink of electronic energy upon the transition. Accepting modes are limited to those whose Franck–Condon factors are appreciable.

The vibrational component of the non-BO transition matrix elements contains a multidimensional Franck–Condon factor. The simplest approach to evaluating the multidimensional Franck–Condon factors is to assume that the ground- and excited-state potential surfaces are harmonic and differ only in their minimum positions by Δ. The vibrational frequencies and normal coordinates are then identical in the ground and excited states, and a system of N vibrational modes can be treated as a collection of N independent pairs of harmonic oscillators. We can safely assume that the molecule is not vibrationally excited in the E_u state because the energy of pump pulse matches to the $0-0$ energy difference between the A_{1g} and E_u states. So the molecule is supposed to be vibrationally unexcited in the initial electronic state of the nonradiative transition. Therefore, the non-BO theory predicts that the accepting or promoting modes can be vibrationally excited in the final state.

First, we would like to discuss the first trend, that the rise is fast for totally symmetric modes, but somewhat delayed for nontotally symmetric modes. In order to be an accepting mode, the mode has to have nonzero Franck–Condon product between $v = 0$ and $v \neq 0$ states. This means that there is a displacement between the potential minima of E_u and B_{1g} states along the vibrational coordinate of the accepting mode; otherwise the Franck–Condon product between $v = 0$ and $v \neq 0$ becomes zero. This is satisfied only for totally symmetric (A_{1g}) modes under the assumptions described above. On the other hand, in order to be a promoting mode, the mode has to have the same symmetric representation as that of the cross product of E_u and B_{1g}, that is, E_u symmetry. In the resonance Raman spectra, we observed A_{1g} and B_{1g} skeletal vibrational modes. Among them, the A_{1g} mode can be an accepting mode, but the B_{1g} mode cannot be an accepting or a promoting mode. Accordingly only the A_{1g} modes can be vibrationally excited after nonradiative transition and the symmetry dependence can be qualitatively explained.

Next we would like to discuss the other trend, which is that the intensity rise gets slower as the frequency of the mode gets lower. We can explain this as follows. In order to receive a certain amount of excess energy, the change of the vibrational quantum number has to be larger for a lower frequency mode. In the range of realistic size of Δ for metalloporphyrins, Franck–Condon product becomes smaller as the change in the vibrational quantum number becomes larger. Therefore, the low frequency modes would be poor acceptor modes because they cannot take up a lot of energy without making their quantum number high. This can be a reasonable explanation for the second trend. For both trends, the non-uniform rise is supposed to reflect the probability for the modes to be an accepting mode.

Anti-Stokes Raman bands due to ethyl substituents showed the delay in intensity rise. This indicates that most of the excess energy is stored in the macrocycle modes and that ethyl modes are less excited shortly after the nonradiative transition to the (d, d) excited state. A similar phenomenon was observed for NiTPP. Figure 7 shows Stokes and anti-Stokes TR[3] spectra of NiTPP at 1-ps following the photoexcitation. The phenyl mode, ϕ_4, was observed at 1599 cm^{-1} in the Stokes spectrum (A), while no prominent anti-Stokes counterpart was observed in the anti-Stokes spectrum (B), suggesting that the ϕ_4 mode is not excited as much as the macrocycle modes. These results show that the peripheral modes are neither efficient accepting nor promoting modes on the nonradiative transition of the nickel porphyrins.

For large molecules with dense vibrational manifolds, the following scheme of the relaxation process involving two temporally distinct steps has been proposed.[1,3]

$$\mathrm{A} \xrightarrow{\text{IVR}} \mathrm{B} \xrightarrow{\text{IET}} \mathrm{C}$$

Here A represents the state initially prepared by optical excitation or nonradiative transition with a non-statistical distribution of vibrational energy, B a state characterized by a Boltzmann distribution of high vibrational energy,[67] and C a thermally equilibrated state at ambient temperature. The validity

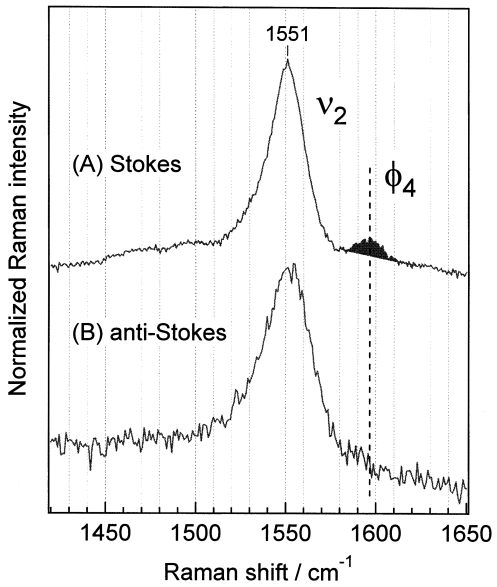

Fig. 7. Stokes (A) and anti-Stokes (B) TR^3 spectra of NiTPP at 1-ps time delay (pump: 532 nm, probe: 458 nm).

of this picture relies on a clear separation in time scales between the intra- and intermolecular energy transfer processes. Indications that these two steps are temporally distinct in complex systems have come mainly from ultrafast transient absorption and emission studies. Mokhtari et al. observed biexponential dynamics for emission bandwidth and band position of dye molecules, which were interpreted as resulting from subpicosecond IVR, followed by an order of magnitude slower IET process.[68] Similar conclusions were reached by several groups in their transient absorption studies of organic dye molecules in solution.[69–72]

In the absence of such a separation, the transfer of energy to the solvent competes with the internal redistribution process, and as a result, the solute may never achieve a Boltzmann distribution of the excess energy. In fact, several recent experiments have suggested that the IVR is not completed within a few picoseconds for large molecules in solutions. For example, time-resolved absorption spectra observed for nascent *trans*-stilbene in the ground electronic state formed via photoisomerization of *cis*-stilbene have shown that the IVR process is not completed in the time range of the *cis* to *trans* photoisomerization (subpicosecond), and non-statistical distributions of vibrational populations persist for several picoseconds.[12,13] From the anti-Stokes Raman spectral changes of *trans*-stilbene in the lowest excited singlet state, the time scale of the IVR process in the S_1 state has been estimated to be of the order of picoseconds.[25,27,28,30] Experimental results from other polyatomic molecules, namely, bacteriorhodopsin,[73] metalloporphyrins,[50–52] and 2-(2-hydroxy-5-methylphenyl)benzotriazole[14] have also suggested that the IVR processes occur in the picosecond range. None of these studies, however, gives concrete information on both the time scale of IVR and the mode specificity. The present experimental data give more direct evidence that the statistical energy distribution has not been achieved in a picosecond time scale for NiOEP.

4 IET of Metalloporphyrins

4.1 NiOEP. To study the IET mechanism, solvent dependence of the time constants of the anti-Stokes kinetics was investigated using deuterated benzene, toluene, deuterated toluene, and tetrahydrofuran (THF). The results are summarized in Table 2. The IET time (τ_1 in Table 2) of NiOEP in the various solvents exhibited no prominent solvent dependence. In solutions, energy transfer to other solute molecules or to solvent molecules has to be considered. The concentration of NiOEP in the present experiments suggests an averaged solute-solute separation of approximately 300 Å. Therefore, the energy transfer to other solute molecules is negligible. This is supported by the observation of similar time constants for the IET upon variation of the concentration by a factor of 10. Generally for liquids, there are three possible mechanisms for the intermolecular energy transfer: (i) direct V → V energy transfer; (ii) through hydrogen bonds; and (iii) through collisional energy transfer or V → T energy transfer. Based on the work by Scherer et al.,[74] the dominant mechanism of energy transfer was suggested to be the last.

In the case of NiOEP investigated here we have found very weak dependence of the τ_1 time constants on solvents which have different spectra of vibrational modes. Although optically active modes are limited in the case of benzene, the substitution of C–H with C–D changes the frequencies of various in-plane skeletal modes in the 400–1600 cm^{-1} region as well as the out-of-plane and their combination modes in the 100–1600 cm^{-1} region.[75] Accordingly, not only the C–H(D) stretching but also the entire vibrational density of states including the low frequency region are significantly influenced by the isotope substitution. Consequently, direct V → V energy transfer does not seem to play a major role in the IET process. The

Table 2. Solvent Dependence of Time Constants for the Temporal Behaviors of the Anti-Stokes ν_4 and ν_7 Bands[a)]

Solvent	ν_4		ν_7		
	τ_1	τ_2	τ_{rise}	τ_1	τ_2
Benzene-h_6	10 ± 2	340 ± 50	2.0 ± 0.4	11 ± 2	330 ± 40
Benzene-d_6	12 ± 2	300 ± 40	2.4 ± 0.5	10 ± 2	350 ± 40
Toluene-h_8	9 ± 2	330 ± 50	2.4 ± 0.8	13 ± 2	320 ± 50
Toluene-d_8	9 ± 2	320 ± 50	2.4 ± 0.6	12 ± 2	310 ± 50

a) All time constants are in picoseconds.
τ_1: IET time constant, τ_2: electronic relaxation time of the (d, d) excited state, τ_{rise}: rise time constant

mechanism (ii) is not the case, because hydrogen bonding is absent in solvents like benzene and toluene. We, therefore, are led to conclude that IET via collisional energy transfer prevails in energy transfer from the excited NiOEP to surrounding solvents.

Iwata and Hamaguchi measured the cooling rates of S_1 *trans*-stilbene in different solvents and found a strong correlation with thermal diffusivities of the bulk solvents.[76] They explained the observed correlation with the idea that the excess energy is first shared by the solute and the nearest solvent molecules within a few picoseconds and that further heat conduction to outer-sphere solvent molecules determines the whole dissipation rate. In contrast, very weak dependence of the cooling rate of NiOEP on solvent was observed in the present study. It may be due to the fact that the thermal diffusivity varies over a range of only ~5% in the present case.

4.2 Water-Soluble Iron Porphyrin. We also tried to measure the kinetics of vibrational relaxation in halogen-containing solvents such as chloroform and dichloromethane, but NiOEP was decomposed in an hour during the TR^3 measurements presumably due to radical reactions. The solubilities of NiOEP in polar solvents were too low to obtain reasonable signal-to-noise ratios of Raman spectra. Thus, the number of solvents which can be used for NiOEP, was limited. Therefore we examined FeTSPP having four sulfophenyl groups at mesocarbons, which make this molecule soluble in polar solvents.[113] The formation of vibrationally excited FeTSPP via internal conversion from the S_1 state to the S_0 state and its subsequent vibrational energy relaxation was monitored by picosecond anti-Stokes resonance Raman intensity changes. We investigated the cooling rates of FeTSPP in three different solvents. One is water and other two are mixed solvents composed of methanol and benzene. In water solution, the anti-Stokes ν_4 band showed a single exponential decay, of which the time constant was 1.9 ± 0.4 ps (Fig. 8). In contrast, the band showed an additional slow decay phase in the mixed solvents. The contribution of the slow phase increased when the volume fraction of benzene increased while the behavior of the fast phase was almost independent of the solvent. Therefore we ascribed the fast phase to the process in which the solute–solvent energy transfer is rate-limiting and the slow phase to the process in which solvent–solvent energy transfer is rate-limiting.

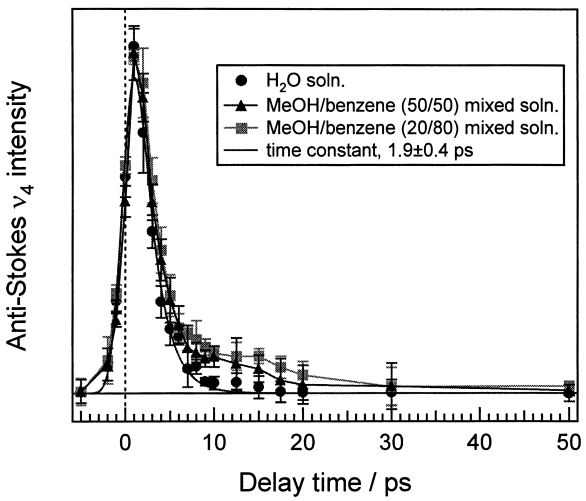

Fig. 8. Temporal changes of the Raman intensity of anti-Stokes ν_4 band of FeTSPP in water (circles) and in mixed solvents composed of methanol and benzene, 50/50 (triangles) and 20/80 (squares) in volume percent.

In order to verify this assignment, we calculated the solvent temperature in the classical thermal diffusion model as proposed by Li and Champion.[77] It is reasonable to assume that the observed intensity decay of the ν_4 mode mainly reflects the IET process, because all of the observed anti-Stokes intensities decayed in a similar manner. Therefore, in the model, we neglect the IVR process in the solute for simplification of the situation. Under such an assumption, the extent of vibrational excitation can be expressed with the internal temperature of the solute. We consider the classical cooling process of a spherical solute with radius, a, in the continuous medium. The cooling of the solute can be described by the surface conductivity between the solute and medium, H, and the thermal diffusivity of the medium, K. We solved an equation of thermal diffusion

$$K\frac{\partial^2(rT)}{\partial r^2} - \frac{\partial(rT)}{\partial t} = 0 \tag{1}$$

with the following boundary conditions

$$\begin{aligned} C_a\frac{\partial T_a}{\partial t} + 4\pi a^2 H(T_a - T) &= 0 \ (\text{at } r = a) \\ C\rho K\frac{\partial T}{\partial r} + H(T_a - T) &= 0 \ (\text{at } r = a) \end{aligned} \tag{2}$$

where T_a and C_a are the temperature and heat capacity of the solute, respectively, and T, C, and ρ are the temperature, heat capacity, and density of the medium, respectively.

Figure 9 shows the normalized solute temperature. The left panel shows a log–log plot of the solute temperature versus delay time, and the right panel shows a linear plot of the same ones. In the early time regime, the cooling is mainly determined by the solute-solvent process and shows exponential decay. On the other hand, in the later time regime, the solvent-solvent process is a rate-limiting step of cooling and the temperature shows diffusive decay ($\sim t^{-3/2}$). The slow component became more prominent when thermal diffusivity of solvent becomes lower (right panel). Accordingly, the model calculation qualitatively reproduces the observed results. This supports the interpretation that the fast component reflects the solute-solvent energy transfer process.

4.3 Mb. Mb is an oxygen-storage protein containing a heme prosthetic group. The heme is embedded within the globin and is linked to it through the proximal histidine. Although a heme and a protein constitute a single molecule, the heme prosthetic group is relatively isolated from the protein and approximates to a heme in a protein matrix. The heme is linked covalently to the surrounding globin through the proximal His. Motion along the Fe–His coordinate is orthogonal to the in-plane mode of the heme and, to a first approximation, they are regarded as being decoupled from the vibrational modes of the porphyrin ring. The heme is maintained in a cav-

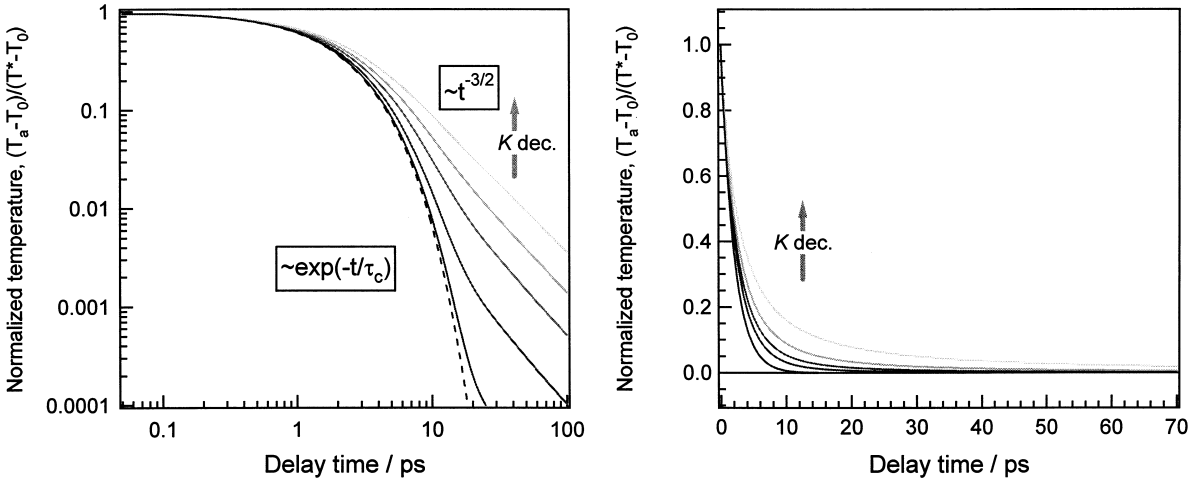

Fig. 9. The plot of normalized solute temperature vs delay time for the classical thermal diffusion model with $a = 0.5$ nm, $C_a = 1.0 \times 10^{-21}$ J/K, and $C_\rho = 4.18$ J/Kcm^3.

ity by approximately 90 van der Waals contacts with the protein.[78] Therefore, the heme can be regarded as a solute molecule dissolved in a "protein solvent".

Figure 10 shows the Stokes time-resolved resonance Raman difference spectra of photodissociated Mb for various values of delay time of the probe pulse with respect to the pump pulse. In these spectra, the contribution of unreacted species has been subtracted. The fraction of photolyzed MbCO was estimated to be 6% based on the intensity loss of the Raman bands of MbCO. The TR^3 spectrum in the 1000 to 1700-cm^{-1} region for a 1-ps delay contains only the bands arising from the in-plane vibrations of heme at 1352 (ν_4), 1560 (ν_2), and 1617 (ν_{10}) cm^{-1}.[37,38] These bands exhibited an appreciable narrowing and frequency upshift in the first few picoseconds, but no further changes occurred after that. The TR^3 spectrum for a 10-ps delay closely resembles the spectrum of deoxyMb, indicating that the photodissociated heme has relaxed to the equilibrium structure within the instrument response time (~2 ps). There is no Raman band that can be assigned to the excited electronic state. The involvement of the excited electronic state in the relaxation pathway remains as a possibility, and there are reports that suggest that this is likely.[46,79,80] However, the results in this work and other studies[49,81] indicate that a majority of the population is directly channeled into the vibrational manifolds of the ground electronic state, and minor channels may lead to an appearance of small amounts of long-lived (ps time scale) intermediate states.[49] The intensity invariance in the spectra for delay times between 5 and 50 ps is consistent with the fact that recombination of CO to the heme takes place in the time regime of microseconds to milliseconds[82] in contrast with the cases for NO and O_2.[82]

The anti-Stokes TR^3 difference spectra of photodissociated MbCO between −5 and 50 ps are shown in Fig. 11. Anti-Stokes intensities are highest at a 1-ps delay, when the ν_3, ν_4, ν_5, ν_6, and ν_7 bands were observed at 1469, 1353, 1118, 783, and 669 cm^{-1}, respectively. These bands lose intensity as the delay time increases and reached their equilibrium intensities at a 10-ps delay.

Figure 12 shows the temporal changes of Stokes (A) and anti-Stokes (B) ν_4 and ν_7 band intensities. The Stokes intensity develops within the instrument response time and remains constant. This is consistent with the photodissociation of CO from the heme taking place within 50 fs[35] and with the fact that the recombination of CO takes place in the time range of microseconds to milliseconds. The anti-Stokes intensity also develops within the instrument response time. The instrument response was deconvoluted from the decay of the anti-Stokes intensity using a Gaussian fit to the cross correlation signal. This analysis enabled us to obtain the decay constants of 1.1 ± 0.6 ps for the ν_4 band and 1.9 ± 0.6 ps for the ν_7 band. Because there is no intensity change in the Stokes ν_4 and ν_7 bands in the 3 to 50-ps time range, the observed intensity decay in the anti-Stokes ν_4 and ν_7 bands can be ascribed to vibrational energy relaxation.

Pioneering work about the energy flow from the heme into the protein matrix was reported by Henry et al.,[78] who carried out molecular dynamics simulations for Mb and cytochrome *c* with initial energy deposits corresponding to optical excitation at both 532 and 355 nm. The simulation predicted a fast initial relaxation phase with decay constants of 1 to 4 ps, followed by a slower relaxation phase with decay constants of 20 to 40 ps. To compare those predictions with the results in this work, it is necessary to estimate the temperature decay rate of the heme. The anti-Stokes/Stokes Raman intensity ratio is determined by the Boltzmann factor for the vibrational mode in question, assuming a statistical distribution of vibrational energy. When the observed kinetics of population decay in vibrationally excited states are converted to temperatures by assuming a Boltzmann distribution, the time constant of 1.1 ± 0.6 ps for the population decay give rise to the time constant of about 2 ps for the temperature decay. This value appears to be close to the value of the fast component predicted by Henry et al.[78] However, the molecular dynamics simulations suggested a ratio of 50:50 for the magnitudes of the fast and the slow components, whereas we did not observe such a large contribution of the slow component in Fig. 12(B). It is noted that the simulation was conducted in vacuo and neglected the effect of the water bath, which works as an extensive thermal sink. In fact, fast heating of water with a time constant of 7.5 ± 2.0 ps was observed for Mb in D_2O.[83] Genberg et al. studied the vibra-

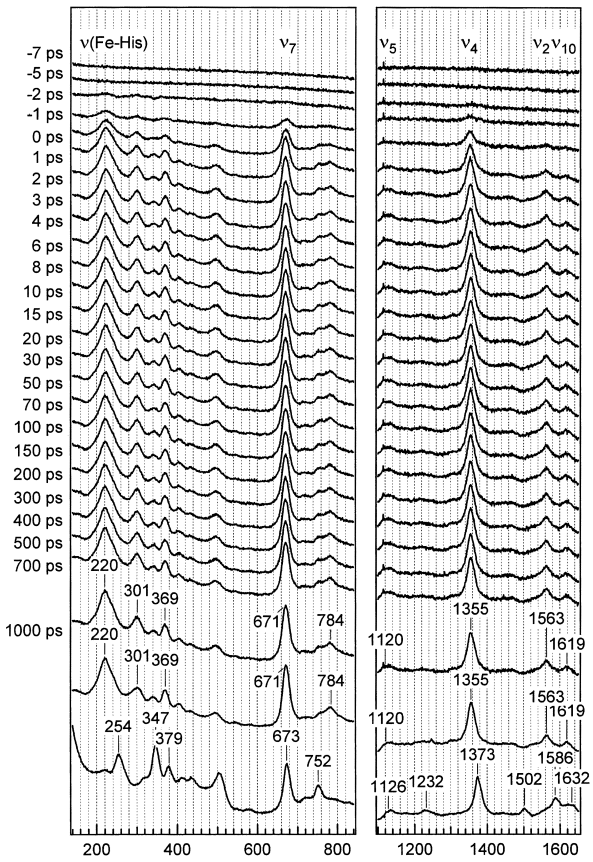

Fig. 10. TR^3 Stokes spectra of photodissociated MbCO in the 140 to 1700-cm^{-1} region. Stokes spectra of the equilibrium deoxyMb and MbCO are depicted at the bottom for comparison. Horse skeletal Mb was dissolved into a buffer (50 mM Tris·HCl, pH 8.0) and filtrated through a 0.45-μm PTFE membrane (Millipore) to make a 300-μM solution. One milliliter of the Mb solution was placed into an airtight NMR tube (10 mmϕ). The remaining oxygen in the solution was removed by more than five cycles of degassing and back-filling with CO. Finally the solution was equilibrated under 1 atm of CO. The samples were reduced with a 5-fold stoichiometric amount of sodium dithionite in a small amount of solution (approximately 50 μL). The sample solution in the cell was continuously spun during the measurements to prevent multiple probing of the same portion of sample. The sample was replaced with a new one every three hours. Sample integrity was confirmed with UV-visible absorption spectra after the TR^3 measurements. The samples of deoxyMb were prepared by the same procedure with MbCO preparation, except for back-filling with N_2 and the equibration of the sample under 1 atm of N_2.

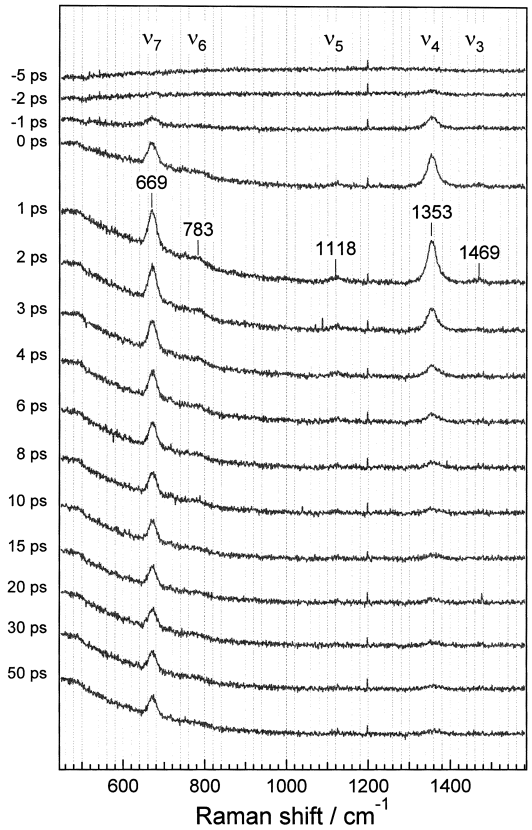

Fig. 11. TR^3 anti-Stokes spectra of photodissociated MbCO in the 450 to 1600-cm^{-1} region (see caption of Fig. 10 for sample preparation).

tional energy relaxation of optically excited hemeproteins by using a transient phase grating technique, and they found that vibrational energy was transferred from the heme to the water interface through the protein matrix in less than 20 ps.[84] A molecular dynamics simulation with the presence of water molecules indicated that the inclusion of water increases the rate of the slower phase in cooling to a 10-ps time scale.[85] Disregarding the effect of the water bath may decelerate the cooling rate of heme, resulting in a larger contribution by the slow component.

Hopkins and his co-workers measured the TR^3 spectra of deoxyHb with a time resolution of 8 ps.[48] Intensity changes of both negative transients in Stokes and positive transients in anti-Stokes showed population changes with a time constant of 2 to 5 ps, to which the 1 to 2-ps decay of Fig. 10 obtained with a higher time resolution is comparable, despite differences in the globin (Mb vs Hb) and phenomena (CO-photodissociation vs electronic excitation). Petrich et al. studied the vibrational relaxation of hemeproteins indirectly using femtosecond Stokes resonance Raman spectroscopy, and they estimated the temperature of heme in HbCO based on the band shift of the ν_4 mode.[45] They concluded that the heme in the HbCO photoproduct was substantially cooled within 10 ps. Li et al. qualitatively analyzed Stokes and anti-Stokes Raman scattering of different hemeproteins to determine the heme vibrational temperature as a function of nanosecond laser flux. They obtained a time constant of about 4 ps for heme cooling.[49] These experimental results on the time scale of vibrational energy relaxation are in agreement with the results of this work.

The fast energy dissipation from the globin to the water bath has also been noted in femtosecond TRIR (time-resolved IR) studies that monitor the heating of water caused by the photoexcitation of deoxyMb.[83] The observed kinetics was fitted with a model having two time constants. The fast component was best fitted by a Gaussian rise function with a time constant

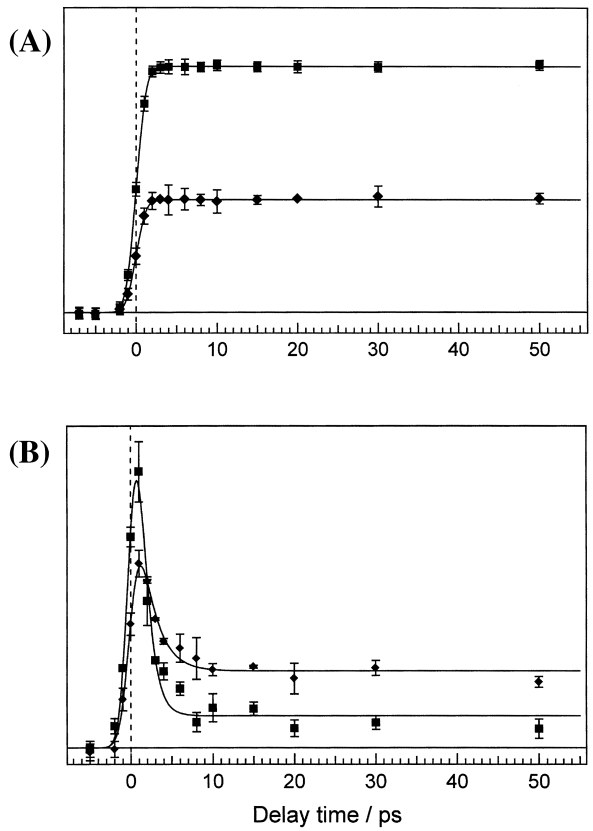

Fig. 12. Temporal changes of the Raman intensity of the Stokes (A) and anti-Stokes (B) ν_4 and ν_7 bands of photodissociated MbCO. In the panel (A), the lines show the results calculated for a step function (assuming an instantaneous rise and very slow decay) convoluted with a Gaussian instrument response function for which the cross correlation time is 2.3 ps. In the panel (B), the solid lines represent fits using an exponential function of the form, $A(\exp(-t/\tau_{decay}) + B)$ (an instantaneous rise and an exponential decay) convoluted with an instrument function as shown in the caption of Fig. 5. The lines shown in this figure were obtained with the parameters of $\tau_{decay} = 1.1 \pm 0.6$ ps and $B = 0.03 \pm 0.01$ for the ν_4 band, and $\tau_{decay} = 1.9 \pm 0.6$ ps and $B = 0.31 \pm 0.02$ for the ν_7 band.

of 7.5 ± 1.5 ps, and the slow component was described by a time constant of ca. 20 ps with 40% of the total amplitude. A comparison of the heme cooling (TR^3) and water heating (TR-IR) studies suggests that there are two channels of energy dissipation from the protein to the water bath. One is a classical diffusion process, and it is responsible for the slow component; the observed time constant is in reasonable agreement with that calculated using the classical diffusion theory. The other is probably through the collective motions of the protein,[83] and it is responsible for the fast component. The time constant of heme cooling (3 ps) is shorter than that of water heating (7.5 ps). This time lag may correspond to the time required for energy propagation via the collective low-frequency modes of the protein. Very recently, Sagnella et al.[86] and Okazaki et al.[87] proposed that a possible doorway for energy release from the vibrationally excited heme involves the interaction of its propionate groups with neighboring solvent molecules.

One-color[88] and two-color[89] infrared pump-infrared probe spectroscopy has been used to determine the vibrational relaxation time (T_1) for the CO stretching vibrations in the unphotolyzed state of MbCO in D_2O at 300 K. Both measurements obtained similar results of 17 ps for T_1 time. The CO T_1 time can be affected by the protein structure:[88] two different conformers of MbCO have significantly different T_1 times. It is interesting to compare the time constants of the vibrational energy relaxations of the heme modes with that of the internal mode of CO bound to the heme. The T_1 of the CO stretch is much longer than the time constants observed for heme cooling in Mb, indicating that there is not efficient intramolecular energy exchange between the bound CO and the porphyrin ring. One reason for the less efficient energy exchange is relatively low frequencies of the other FeCO modes (577 and 512 cm^{-1} for the FeCO bend and FeC stretch of MbCO, respectively). These frequencies imply that at least three quanta are required to come within a few hundred wavenumbers of the energy of the CO stretching mode. A pathway involving the transfer of the CO vibrational energy into other FeCO modes therefore requires large anharmonic coupling.

There are studies on the vibrational energy relaxation of CO in the photolyzed state, where CO is not covalently attached but is trapped within a docking site. The structure and dynamics of the photolyzed state have recently been probed using X-ray diffraction,[90–93] vibrational spectroscopy,[94,95] and computer simulation.[96–98] Photolysis of MbCO produces a significant population of CO in its excited vibrational state. Based on time-resolved mid-IR absorbance measurements, T_1 time of 600 ± 150 ps was determined.[99] Because the photodissociated CO has no covalent interactions, its T_1 time is significantly longer than that observed in the bound state. Measurement of this relaxation time will clarify the role of the "protein solvent" in the relaxation of CO. The Landau–Teller theory predicted that the relaxation rate of $1/T_1$ is expressed remarkably well by the Fourier component of time-dependent friction evaluated at the frequency of the oscillator,[100] which is connected to the time correlation function of the fluctuating force along the vibrational coordinate by the second fluctuation–dissipation theorem. Sagnella et al. computed the influence spectrum, which is practically the distribution of the square of the coupling constants between the CO stretch and the bath modes as a function of frequency.[99] In their simulations, the relaxation was dominated by short-ranged van der Waals interactions with the residues forming the inner wall of the heme pocket of Mb. The data suggests that the mechanism for the vibrational relaxation of CO in Mb takes place through successive, noncorrelated collisions with the pocket residues, acting as a first solvation shell to the CO molecule.

The exchange mechanism of vibrational energy within proteins is little understood. Several time-resolved experiments were performed with picosecond and femtosecond infrared pulses to study the dissipation of locally deposited energy in the protein backbone (amide I mode).[101–103] The amide I vibrational mode involves mainly the C=O stretching motion of the peptide backbone containing a small amount of contributions from the CN and NH motions.[104] Because the amide I vibrational mode is a strong infrared absorber, this band is ideal for mid-infrared transient absorption ("pump-probe") measure-

ments. Mb is almost entirely α helical in the secondary structure, and it shows the amide I band centered near 1650 cm^{-1} in D_2O. Peterson et al. carried out mid-infrared transient absorption measurements on the amide I band of Mb over a wide temperature range (6 to 310 K).[102] The temperature dependence of the vibrational relaxation in the solvent mixture is slight, changing from 1.9 ± 0.2 ps below 100 K to 1.2 ± 0.2 ps at 310 K. Tokmakoff et al.[105] and Kenkre et al.[106] gave detailed discussions on the temperature dependencies of vibrational relaxation. In general, if two or more low-frequency bath modes are involved, vibrational relaxation has a significant temperature dependence since, at higher temperatures, the thermal population of the bath modes increase the relaxation rate through a stimulated process. The lack of a strong temperature dependence is indicative of a low-order relaxation process where energy is transferred into the high-energy modes of the system rather than directly to the low-energy solvent or protein "bath" modes. Femtosecond pump-probe measurements by Hamm et al. on small proteins, including apamin, scyllatoxin, and bovine pancreatic tripsin inhibitor, each of which contains both of the α-helix and β-sheet structures in different proportions, show an identical lifetime of 1.2 ps for amide I.[101] Despite the differences in their sizes and secondary structures, the amide I relaxation dynamics observed in both of these studies are essentially the same and appear to be fundamental features of the amide I mode in polypeptides and proteins. It is interesting that the heme and the amide I modes show similar vibrational lifetimes,[103] although the coincidence may be accidental.

Concerning solute-solvent energy transfer, we studied a role of low frequency vibrations of globular proteins. Globular proteins have delocalized skeletal vibrational modes with low frequencies. These delocalized low frequency modes have been thought to act as doorway states and to accelerate the rate of the energy transfer.[107,108] We compared the cooling time constants of FePPIX embedded in protein (Mb) and in an organic solvent (DMF). No difference was observed between time constants for FePPIX in Mb (1.1 ± 0.6 ps) and in DMF (1.4 ± 0.5 ps, data not shown). This means that low frequency vibrations of protein contribute little to the energy release from FePPIX. This observation also suggests that V–V resonance energy transfer is not predominant and that V–T type energy transfer would be a dominant mechanism.

5 Summary and Perspectives

We have successfully applied picosecond TR^3 spectroscopy to explore the vibrational dynamics of metalloporphyrins in organic solvents and protein matrix, and demonstrated that this technique is powerful to study the mechanism of vibrational relaxation owing to high time resolution and mode selectivity.

Our recent studies revealed that IET of metalloporphyrins in a condensed phase takes place in picoseconds and that the solute-solvent process mainly limits the transfer rate. It was also shown that the IVR of metalloporphyrins in a condensed phase are not completed in a picosecond: in NiOEP, non-uniform intensity rises of anti-Stokes Raman bands were observed; in Mb, rates of vibrational relaxation of the heme in-plane modes are much different from that of the internal mode of CO bound to the heme. We found that the IVR rate is comparable to the IET rate for metalloporphyrins in solution. This conclusion would be applied to other planar conjugated molecules like phthalocyanine and chlorophyll and their derivatives. It is interesting to discuss on the extent to which the knowledge obtained from the studies on the VER in metalloporphyrins is general to other systems. We note that metalloporphyrins are not peculiar molecules with regard to anharmonicity of molecular vibrations: in the RR spectra of NiOEP, for example, about 90 overtone and combination bands were observed,[36] suggesting that anharmonic couplings among the vibrational modes are by no means small. Therefore, the comparable IVR rate to the IET rate would be expected in other large molecules in solution. However, it would be premature to deduce some general conclusion from the results for metalloporphyrins. It should be noted that the present study demonstrates the importance of examining the *mode dependence* of vibrational energy relaxation to elucidate the mechanism of VER in a condensed phase.

Studies of vibrational energy relaxation of electronically excited molecules in solution phases have important implications for understanding mode-specificity in ultrafast photochemical reactions as well as for understanding the nature of solute-solvent interactions. Ultrafast electron transfer reaction is a typical example in which intramolecular vibrations play an important role. Recently, it was found that vibrational relaxation times (on the order of several picoseconds) are much slower than the electron transfer (~100 fs) in cyanide bridged mixed-valence transition metal dimers.[109] Thus, the general assumption that reactions proceed out of a thermally equilibrated excited state is not correct. Under such conditions, reaction rates may be faster than that predicted by theory. Understanding of intramolecular vibrational energy relaxation is required for improvement of the theory. On the other hand, intermolecular vibrational energy relaxation is connected with solute-solvent interactions. Recently, intermolecular interaction between ionic solute and polar solvents has been discussed in terms of vibrational relaxation rates of the solute.[20,110–112] Vibrational energy relaxation gives us great insight into understanding of nuclear dynamics with many degrees of freedom.

The authors thank Dr. Yuki Uesugi for her contribution to the development of the picosecond time-resolved resonance Raman apparatus used in this study. This work was supported by Grants-in-Aid to Y. M. (097404481 and 11740339) and ones to T. K. (12045264 and 13308039) from the Ministry of Education, Culture, Sports, Science and Technology.

References

1 T. Elsaesser and W. Kaiser, *Ann. Rev. Phys. Chem.*, **42**, 83 (1991).

2 J. C. Owrutsky, D. Raftery, and R. M. Hochstrasser, *Ann. Rev. Phys. Chem.*, **45**, 519 (1994).

3 A. Seilmeier and W. Kaiser, Ultrafast Vibrational Energy Transfer in Liquids, in "Ultrashort laser pulses, generation and applications," 2nd ed, ed by W. Kaiser, Springer-Verlag, Berlin (1993), Vol. 60, p. 279.

4 G. W. Robinson and R. P. Frosch, *J. Chem. Phys.*, **37**, 1962 (1962).

5 S. H. Lin, *J. Chem. Phys.*, **44**, 3759 (1966).

6 M. Bixon and J. Jortner, *J. Chem. Phys.*, **48**, 715 (1968).

7 The term of IVR has been used to describe the transfer of energy from prepared initial state to other isoenergetic state in the absence of collisions for isolated molecules in the field of gas phase spectroscopy. In liquid state, unlike gas phase IVR, the modes are far enough apart to be well defined eigenstates in the isolate molecules. In addition, the solvent provides the coupling and energy bath needed to make transitions. For example, Bout et al. [*Chem. Phys. Lett.*, **229**, 87 (1994)] referred to the population transfer to energetically close states within *kT* as solvent-assisted IVR. The solvent origin on vibrational energy redistribution is not involved in the description of IVR in gas phase spectroscopy. While recognizing this distinction, in the present paper, we use the definition generally accepted in the field of liquid state spectroscopy, that is, the intramolecular population transfer to nearly isoenergetic states towards statistical distribution of the excess energy.

8 X. Hong, S. Chen, and D. D. Dlott, *J .Phys. Chem.*, **99**, 9102 (1995).

9 H. Graener, M. Hofmann, and R. Zurl, *J. Phys. Chem. B*, **101**, 1745 (1997).

10 J. Deak, L. K. Iwaki, and D. D. Dlott, *Chem. Phys. Lett.*, **293**, 405 (1998).

11 T. Elsaesser, F. Larmer, W. Kaiser, B. Dick, M. Niemeyer, and W. Luttke, *Chem. Phys.*, **126**, 405 (1988).

12 R. J. Sension, A. Z. Szarka, and R. M. Hochstrasser, *J. Chem. Phys.*, **97**, 5239 (1992).

13 R. J. Sension, S. T. Repinec, A. Z. Szarka, and R. M. Hochstrasser, *J. Chem. Phys.*, **98**, 6291 (1993).

14 K. Lenz, M. Preiffer, A. Lau, and T. Elsaesser, *Chem. Phys. Lett.*, **229**, 340 (1994).

15 K. Wynne and R. M. Hochstrasser, *Chem. Phys.*, **193**, 211 (1995).

16 P. Hamm, M. Zurek, W. Mantele, M. Meyer, H. Scheer, and W. Zinth, *Proc. Natl. Acad. Sci. U.S.A.*, **92**, 1826 (1995).

17 P. Hamm, S. Wiemann, M. Zurek, and W. Zinth, *Opt. Lett.*, **19**, 1642 (1994).

18 B. B. Akhremitchev, C. Wang, and G. C. Walker, *Rev. Sci. Inst.*, **67**, 3799 (1996).

19 H. Okamoto and M. Tasumi, *Chem. Phys. Lett.*, **256**, 502 (1996).

20 P. Hamm, M. Lim, and R. M. Hochstrasser, *J. Chem. Phys.*, **107**, 10523 (1997).

21 H. Okamoto, *Chem. Phys. Lett.*, **283**, 33 (1998).

22 H. Okamoto, T. Nakabayashi, and M. Tasumi, *J. Phys. Chem. A*, **101**, 3488 (1997).

23 K. T. Schomacker, O. Bangcharoenpaurpong, and P. M. Champion, *J. Chem. Phys.*, **80**, 4701 (1984).

24 J. Qian, S. L. Schultz, G. R. Bradburn, and J. M. Jean, *J. Phys. Chem.*, **97**, 10638 (1993).

25 J. Qian, S. L. Schultz, and J. M. Jean, *Chem. Phys. Lett.*, **233**, 9 (1995).

26 S. Sato and T. Kitagawa, *Appl. Phys. B*, **59**, 415 (1994).

27 S. L. Schultz, J. Qian, and J. M. Jean, *J. Phys. Chem. A*, **101**, 1000 (1997).

28 T. Nakabayashi, H. Okamoto, and M. Tasumi, *J. Phys. Chem. A*, **101**, 7189 (1997).

29 T. Nakabayashi, H. Okamoto, and M. Tasumi, *J. Phys. Chem. A*, **101**, 3494 (1997).

30 T. Nakabayashi, H. Okamoto, and M. Tasumi, *J. Phys. Chem. A*, **102**, 9686 (1998).

31 Y. Mizutani, Y. Uesugi, and T. Kitagawa, *J. Chem. Phys.*, **111**, 8950 (1999).

32 D. Kim, C. Kirmaier, and D. Holten, *Chem. Phys.*, **75**, 305 (1983).

33 J. Rodriguez and D. Holten, *J. Chem. Phys.*, **91**, 3525 (1989).

34 B. I. Greene, R. M. Hochstrasser, R. B. Weisman, and W. A. Eaton, *Proc. Natl. Acad. Sci. U.S.A.*, **75**, 5255 (1978).

35 J. W. Petrich, C. Poyart, and J. L. Martin, *Biochemistry*, **27**, 4049 (1988).

36 T. Kitagawa, M. Abe, and H. Ogoshi, *J. Chem. Phys.*, **69**, 4516 (1978).

37 M. Abe, T. Kitagawa, and Y. Kyogoku, *J. Chem. Phys.*, **69**, 4526 (1978).

38 X.-Y. Li, R. S. Czernucszewicz, J. R. Kincaid, P. Stein, and T. G. Spiro, *J. Phys. Chem.*, **94**, 47 (1990).

39 X.-Y. Li, R. S. Czernucszewicz, J. R. Kincaid, and T. G. Spiro, *J. Am. Chem. Soc.*, **111**, 7012 (1989).

40 U. Even, J. Magen, J. Jortner, and H. Levanon, *J. Am. Chem. Soc.*, **103**, 4583 (1981).

41 U. Even, J. Magen, J. Jortner, and H. Levanon, *J. Chem. Phys.*, **76**, 5684 (1982).

42 U. Even, J. Magen, J. Jortner, J. Friedman, and H. Levanon, *J. Chem. Phys.*, **77**, 4374 (1982).

43 U. Even, J. Magen, and J. Jortner, *J. Chem. Phys.*, **77**, 4384 (1982).

44 U. Even and J. Jortner, *J. Chem. Phys.*, **77**, 4391 (1982).

45 J. W. Petrich, J. L. Martin, D. Houde, C. Poyart, and A. Orszag, *Biochemistry*, **26**, 7914 (1987).

46 J. W. Petrich and J. L. Martin, *Chem. Phys.*, **131**, 31 (1989).

47 R. Lingle, Jr., X. Xu, H. Zhu, S.-C. Yu, and J. B. Hopkins, *J. Am. Chem. Soc.*, **113**, 3992 (1991).

48 R. Lingle, Jr., X. Xu, H. Zhu, S.-C. Yu, and J. B. Hopkins, *J. Phys. Chem.*, **95**, 9320 (1991).

49 P. Li, J. T. Sage, and P. M. Champion, *J. Chem. Phys.*, **97**, 3214 (1992).

50 R. G. Alden, M. C. Schneebeck, M. R. Ondrias, S. H. Courtney, and J. M. Friedman, *J. Raman Spectrosc.*, **23**, 569 (1992).

51 M. C. Schneebeck, L. E. Vigil, and M. R. Ondrias, *Chem. Phys. Lett.*, **215**, 251 (1993).

52 M. C. Simpson, E. S. Peterson, C. F. Shannon, D. D. Eads, J. M. Friedman, C. M. Cheatum, and M. R. Ondrias, *J. Am. Chem. Soc.*, **119**, 5110 (1997).

53 Y. Mizutani and T. Kitagawa, *Science*, **278**, 443 (1997).

54 H. Hamaguchi and T. L. Gustafson, *Ann. Rev. Phys. Chem.*, **45**, 593 (1994).

55 Y. Uesugi, Y. Mizutani, and T. Kitagawa, *Rev. Sci. Instrum.*, **68**, 4001 (1997).

56 Y. Mizutani and T. Kitagawa, *Chem. Rec.*, **1**, 258 (2001).

57 S. Kaminaka and T. Kitagawa, *Appl. Spectrosc.*, **49**, 685 (1995).

58 Y. Mizutani, *J. Chem. Phys.*, **109**, 9197 (1998).

59 We adopt the vibrational assignments of NiOEP given by Ref. 38.

60 S. H. Courtney, T. M. Jedju, J. M. Friedman, L. Rothberg, R. G. Alden, M. S. Park, and M. R. Ondrias, *J. Opt. Soc. Am. B*, **7**, 1610 (1990).

61 R. E. Hester, P. Matousek, J. N. Moore, A. W. Parker, W. T. Toner, and M. Towrie, *Chem. Phys. Lett.*, **208**, 471 (1993).

62 K. Iwata and H. Hamaguchi, *Chem. Phys. Lett.*, **196**, 462

(1992).

63 W. L. Weaver, L. A. Huston, K. Iwata, and T. L. Gustafson, *J. Phys. Chem.*, **96**, 8956 (1992).

64 P. Hamm, S. M. Ohline, and W. Zinth, *J. Chem. Phys.*, **106**, 519 (1997).

65 N. H. Gottfried and W. Kaiser, *Chem. Phys. Lett.*, **101**, 331 (1983).

66 The intramode randomization model leads to the conclusion of nonstatistical distribution in the vibrational manifolds in the first few picoseconds, even if the first-order expression is inappropriate for NiOEP. When the first-order expression is inappropriate, the anti-Stokes Raman cross sections except for the transition of $v = 1 \rightarrow 0$ could be negligibly small. But, in this case, the initial temperature as high as 1500 K is necessary to reproduce the observed delay of the intensity rise of the anti-Stokes ν_7 band. The temperature of 1500 K is much higher than the temperature that is calculated under the assumption that the excess energy is partitioned among all modes equally as a result of complete IVR (670 K).

67 A large molecule photoexcited with high energy behaves as if it had a high temperature, although distribution of a total vibrational energy created by photoexcitation is very different from that created by thermal excitation (canonical distribution). Each fundamental mode with frequency $\nu_i < 3000$ cm^{-1} may be considered as a small subsystem of the molecular system of vibrational quantum states. In the case that the energy of the quantum state $h\nu_i$ of the subsystem is small compared to the total energy, the occupation probability of the subsystem is given by $N(\nu_i) = \exp(-h\nu_i/kT)$ in a good approximation. The system, therefore, can be characterized by high "temperature" if the total energy is statistically redistributed over a very large number of isoenergetic states (microcanonical distribution). Kaiser and co-workers called this "internal temperature" [*Chem. Phys. Lett.*, **111**, 326 (1984)].

68 A. Mokhtari, J. Chesnoy, and A. Laubereau, *Chem. Phys. Lett.*, **155**, 593 (1989).

69 F. Wondrazek, A. Seilmeier, and W. Kaiser, *Chem. Phys. Lett.*, **104**, 121 (1984).

70 W. Wild, A. Seilmeier, N. H. Gottfried, and W. Kaiser, *Chem. Phys. Lett.*, **119**, 259 (1985).

71 A. M. Weiner and E. P. Ippen, *Chem. Phys. Lett.*, **114**, 456 (1985).

72 F. Laermer, T. Elsaesser, and W. Kaiser, *Chem. Phys. Lett.*, **156**, 381 (1989).

73 A. P. Shreve and R. A. Mathies, *J. Phys. Chem.*, **99**, 7285 (1995).

74 P. O. J. Scherer, A. Seilmeier, and W. Kaiser, *J. Chem. Phys.*, **83**, 3948 (1985).

75 G. Herzberg, in "Molecular Spectra and Molecular Structure II. Infrared and Raman Spectra of Polyatomic Molecules," reprint ed, Krieger Publishing Company, Malabar, FL (1991), p. 362.

76 K. Iwata and H. Hamaguchi, *J. Phys. Chem. A*, **101**, 632 (1997).

77 P. Li and P. M. Champion, *Biophys. J.*, **66**, 430 (1994).

78 E. R. Henry, W. A. Eaton, and R. M. Hochstrasser, *Proc. Natl. Acad. Sci. U.S.A.*, **83**, 8982 (1986).

79 M. Lim, T. A. Jackson, and P. A. Anfinrud, *J. Phys. Chem.*, **100**, 12043 (1996).

80 P. A. Cornelius, A. W. Steele, D. A. Chernoff, and R. M. Hochstrasser, *Proc. Natl. Acad. Sci. U.S.A.*, **78**, 7526 (1981).

81 F. Rosca, A. T. N. Kumar, X. Ye, T. Sjodin, A. A. Demidov, and P. M. Champion, *J. Phys. Chem. A*, **104**, 4280 (2000).

82 Q. H. Gibson, J. S. Olson, R. E. McKinnie, and R. J. Rohlfs, *J. Biol. Chem.*, **261**, 10228 (1986).

83 T. Lian, B. Locke, Y. Kholodenko, and R. M. Hochstrasser, *J. Phys. Chem.*, **98**, 11648 (1994).

84 L. Genberg, F. Heisel, G. McLendon, and R. J. D. Miller, *J. Phys. Chem.*, **91**, 5521 (1987).

85 R. J. D. Miller, *Ann. Rev. Phys. Chem.*, **42**, 581 (1994).

86 D. E. Sagnella, J. E. Straub, and D. Thirumalai, *J. Chem. Phys.*, **113**, 7702 (2000).

87 I. Okazaki, Y. Hara, and M. Nagaoka, *Chem. Phys. Lett.*, **337**, 151 (2001).

88 J. R. Hill, A. Tokmakoff, K. A. Peterson, B. Sauter, D. Zimdars, D. D. Dlott, and M. D. Fayer, *J. Phys. Chem.*, **98**, 11213 (1994).

89 J. C. Owrutsky, M. Li, B. Locke, and R. M. Hochstrasser, *J. Phys. Chem.*, **99**, 4842 (1995).

90 I. Schlichting, J. Berendzen, G. N. Phillips, Jr., and R. M. Sweet, *Nature*, **371**, 808 (1994).

91 T. Y. Teng, V. Srajer, and K. Moffat, *Nat. Struct. Biol.*, **1**, 701 (1994).

92 H. Hartmann, S. Zimser, P. Komninos, R. T. Scheinder, G. U. Nienhaus, and F. Parak, *Proc. Natl. Acad. Sci. U.S.A.*, **93**, 7013 (1996).

93 V. Srajer, T. Teng, T. Ursby, C. Pradervand, Z. Ren, S. Adachi, W. Schildkamp, D. Bourgeois, M. Wulff, and K. Moffat, *Science*, **274**, 1726 (1996).

94 M. Lim, T. A. Jackson, and P. A. Anfinrud, *Science*, **269**, 962 (1995).

95 M. Lim, T. A. Jackson, and P. A. Anfinrud, *Nat. Struct. Biol.*, **4**, 209 (1997).

96 J. E. Straub and M. Karplus, *Chem. Phys.*, **158**, 221 (1991).

97 J. Ma, S. Huo, and J. E. Straub, *J. Am. Chem. Soc.*, **119**, 4355 (1997).

98 D. Vitkup, G. A. Petsko, and M. Karplus, *Nat. Struct. Biol.*, **4**, 202 (1997).

99 D. E. Sagnella, J. E. Straub, T. A. Jackson, M. Lim, and P. A. Anfinrud, *Pro. Natl. Acad. Sci. U.S.A.*, **96**, 14324 (1999).

100 R. M. Whitnell, K. R. Wilson, and J. T. Hynes, *J. Phys. Chem.*, **94**, 8625 (1990).

101 P. Hamm, M. Lim, and R. M. Hochstrasser, *J. Phys. Chem. B*, **102**, 6123 (1998).

102 K. A. Peterson, C. W. Rella, J. R. Engholm, and H. A. Schwettman, *J. Phys. Chem. B*, **103**, 557 (1999).

103 A. Xie, L. van der Meer, W. Hoff, and R. H. Austin, *Phys. Rev. Lett.*, **84**, 5435 (2000).

104 T. Miyazawa, T. Shimanouchi, and S. Mizushima, *J. Chem. Phys.*, **29**, 611 (1958).

105 A. Tokmakoff, B. Sauter, and M. D. Feyer, *J. Chem. Phys.*, **100**, 9035 (1994).

106 V. M. Kenkre, A. Tokmakoff, and M. D. Feyer, *J. Chem. Phys.*, **101**, 10618 (1994).

107 D. D. Dlott, *J. Opt. Soc. Am. B*, **7**, 1638 (1990).

108 R. J. D. Miller, *Ann. Rev. Phys. Chem.*, **42**, 581 (1991).

109 S. K. Doorn, R. B. Dyer, P. O. Stoutland, and W. H. Woodruff, *J. Am. Chem. Soc.*, **115**, 6398 (1993).

110 A. E. Johnson, N. E. Levinger, and P. F. Barbara, *J. Phys. Chem.*, **96**, 7841 (1992).

111 M. Li, J. Owrutsky, M. Sarisky, J. P. Culver, A. Yodh, and R. M. Hochstrasser, *J. Chem. Phys.*, **98**, 5499 (1993).

112 M. Shiga and S. Okazaki, *J. Chem. Phys.*, **111**, 5390 (1999).

113 Y. Mizutani and T. Kitagawa, *J. Mol. Lig.*, **90**, 233 (2001).

Yasuhisa Mizutani was born in Mie, Japan, in 1964. He earned his B. Eng. and M. Eng. degrees in 1987 and 1989, respectively, from Kyoto University, working with Prof. Koichiro Nakanishi. He received his Ph. D. degree from the Graduate University for Advanced Studies in 1992 under the supervision of Prof. Teizo Kitagawa. After that, he did postdoctoral works at Institute for Molecular Science and at the University of Pennsylvania, where he worked with Prof. Robin M. Hochstrasser. In 1994, he joined the faculty at Institute for Molecular Science, as a research associate of the research group of Prof. Teizo Kitagawa. He has been an associate professor of Molecular Photoscience Reserch Center at Kobe University since June 2001. His research interests include dynamical aspects of chemical reaction in liquids and proteins and spectroscopic approaches to them.

Teizo Kitagawa was born in Kyoto, Japan in 1940. He graduated from the engineering department of Osaka University in 1963, and received his M. Sci. and Ph. D. degrees in 1965 and 1969, respectively from Osaka University, under the supervision of Prof. Tatsuo Miyazawa. He became a research associate of Institute for Protein Research, Osaka University in 1966, an associate professor of Medical School of Osaka University in 1980, and a full professor of Institute for Molecular Science in 1983. During the research associate period, he studied vibrational spectra of polymer crystals and ralated solid-state properties including neutron inelastic scattering and also worked as a postdoctral fellow for Prof. Bryce L. Crawford of University of Minnesota for studies of liquid dynamics using ATR spectroscopy. Since coming back from USA, he has studied dynamic structures-function relationship of proteins using vibrational spectroscopy.